Solar Energy Vol. 42, No. 3, pp. 209–220, 1989
Printed in the U.S.A.

0038–092X/89 $3.00 + .00

COMPARISON OF THEORETICAL MODELS OF PHASE-CHANGE AND SENSIBLE HEAT STORAGE FOR AIR AND WATER-BASED SOLAR HEATING SYSTEMS

A. A. GHONEIM
Laboratory of Physics, Mathematical Eng. and Eng. Physics Dept., Faculty of Engineering,
University of Alexandria, Alexandria, Egypt

1. INTRODUCTION

The use of phase-change materials (PCMs) for thermal energy storage in solar heating and cooling systems has received considerable attention. The motivation for using phase-change energy storage (PCES) is the reduction in storage volume which can be achieved compared to sensible heat storage. Using a one-dimensional model with an infinite heat transfer coefficient between the air and storage medium, Morrison, *et al.*[1] have shown that air-based solar systems utilizing sodium sulphate decahydrate ($Na_2 SO_4.10 H_2O$) as a storage medium require roughly one-fourth the storage volume of a pebble bed. For paraffin wax, the required volume increases to approximately one-half the storage volume of a pebble bed. Their results are based on a seven month heating season from October 1 to May 1 for Madison, WI and Albuquerque, NM.

For liquid-based systems, their results showed that a system utilizing paraffin wax may require a slightly larger storage volume than a system of comparable performance with a water tank. On the other hand, systems utilizing $Na_2 SO_4.10 H_2O$ require roughly one-half the storage volume of a conventional water tank system.

The model used by Morrison *et al.* to describe the performance of PCES unit is based on the following assumptions:

- the PCM behaves ideally, i.e. such phenomena as property degradation, supercooling and crystalization are not accounted for, and the phase-change material is assumed to have definite melting temperature
- infinite thermal conductivity for the PCM in the direction normal to the flow (radial direction); this assumption requires that Biot number is sufficiently low such that the temperature gradients in the storage material normal to the flow direction can be ignored
- heat losses from the storage unit to the surroundings are negligible
- zero thermal conductivity for the PCM in the direction parallel to the flow (axial direction)
- the number of transfer units of the storage unit, NTU, is sufficiently large so that the local film temperature difference between the fluid and the PCM can be ignored

In order to test the validity of the first assumption, the effect of semi-congruent melting on system performance was examined in [2]. It was found that a semi-congruent melting of the PCM over a temperature band of up to ±8°C around the nominal melting temperature has only a slight effect on system performance. Even so, the present study takes this effect into consideration.

The main objectives of the present study are

1. To develop a model of PCES which considers
   i) the heat losses from the storage unit,
   ii) the axial conduction in the storage material,
   iii) the radial conduction in the storage material (i.e. the thermal conductivity of the storage material in the radial direction is finite), and
   iv) the local film temperature difference between the fluid and the PCM.
2. To study the effect of assumptions in the models of earlier studies on both the solar fraction (the fraction of the load met by solar energy), and the required storage capacities.

The thermal properties of the storage media used in the present study are given in Table 1.

2. CONFIGURATION OF THE STORAGE VESSEL

Figure 1.1 shows the configuration chosen for the storage vessel. It consists of a vessel packed in the vertical direction with cylindrical tubes. The storage material is inside the tubes and the heat transfer fluid flows parallel to it. To have as much phase-change material as possible, the vessel must be closely packed. The void fraction (the ratio between the fluid volume and the storage tank volume) is assumed to be equal to 0.3. The inside volume and inside surface area of the tank are respectively given by V_t and A_t. The number of cylinders inside the vessel is N_c. The radius of the cylinder tubes is R_c, the length of the cylinders as well as the inside height of the vessel is given by L. R_c is set to 0.02 m and L is set to 2.0 m so that $R_c/L = 0.01$. This ratio is small enough to minimize radial heat conduction in the storage material.

3. ANALYSIS

The thermal energy storage in PCM makes use of the latent heat of the material. The change of state

Table 1. Thermal properties of storage media[3]

Properties	P116 Wax	Medicinal Paraffin	$Na_2SO_4.10H_2O$	Rock
c_s(kJ/kg K)	2.89	2.3	1.92	.84
c_l(kJ/kg K)	+++	2.2	3.26	—
k_s(kJ/m h K)	.497	.5	1.85	.45
k_l(kJ/m h K)	+++	2.1	+++	—
T_{m1}(°C)	46.7	40	32	—
T_{m2}(°C)	+++	44	+++	—
h_{sl}(kJ/kg)	209	146	251	—
ρ_s(kg/m^3)	786	830	1460	2400
ρ_l(kg/m^3)	+++	+++	1330	—

+++ assumed equal to corresponding value for solid phase

results in a moving boundary: on one side of the interface the material is solid, while on the other side it is liquid. This class of problem is known as "Stefan" problems. The problem of tracing the interface can be eliminated by using the specific enthalpy (h) rather than temperature as the dependent variable. The relations between the enthalpy (h) and the temperature (T) for different ranges are as follows:

$$h(T) = c_s T \quad \text{for} \quad T < T_{m1} \tag{1}$$

$$h(T) = C_s T_{m1} + \frac{h_{sl}(T - T_{m1})}{\Delta T_m} \text{ for } T_{m1} \le T \le T_{m2} \tag{2}$$

and

$$h(T) = c_l T + h_{sl} + C_s T_{m1} - C_l T_{m2} \tag{3}$$

where T_{m1} and T_{m2} are respectively, the lower and upper boundary of the transition range, $\Delta T_m = T_{m2} - T_{m1}$, h_{sl} is the latent heat of the phase-change material, c_s specific heat in the solid range, and c_l the specific heat in the liquid range. The problem can be further simplified by using the non-dimensional enthalpy, H^*, which is given by

$$H^* = \frac{h - h_{m1}}{h_{sl}} \tag{4}$$

and the non-dimensional temperature, θ, where

$$\theta = \frac{c_s(T - T_{m1})}{h_{sl}} \quad \text{for} \quad T < T_{m1} \tag{5}$$

and

$$\theta = \frac{c_l(T - T_{m1})}{h_{sl}} \quad \text{for} \quad T \ge T_{m1} \tag{6}$$

The number of axial elements inside the cylinder is M, and the number of radial elements is N + 1 (N elements of the storage material and one fluid element). Considering a cylindrical quantity of PCM (Fig. 1.2), which is a part of the cylinder, taking a control

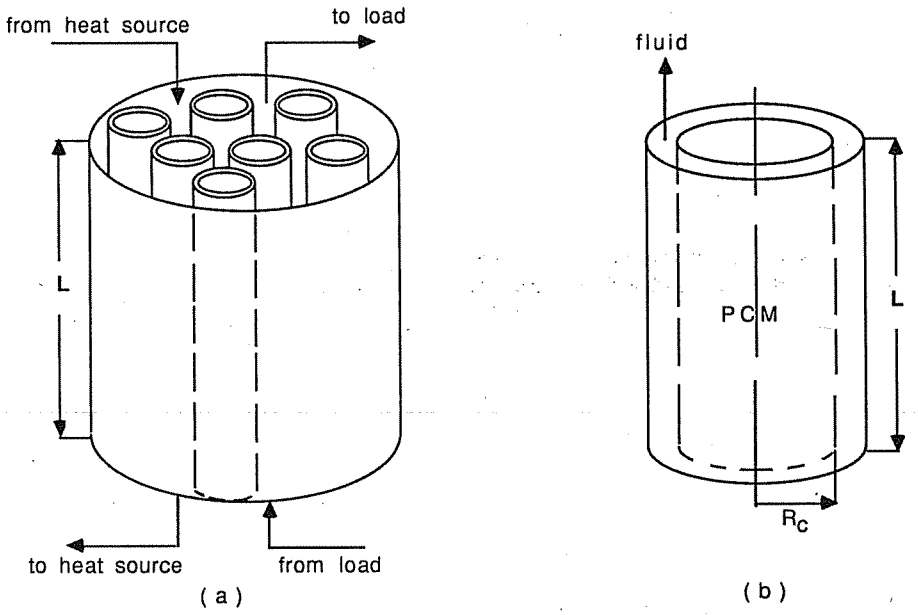

Fig. 1. a) The cylinder-packed vessel; b) the model for one cylinder.

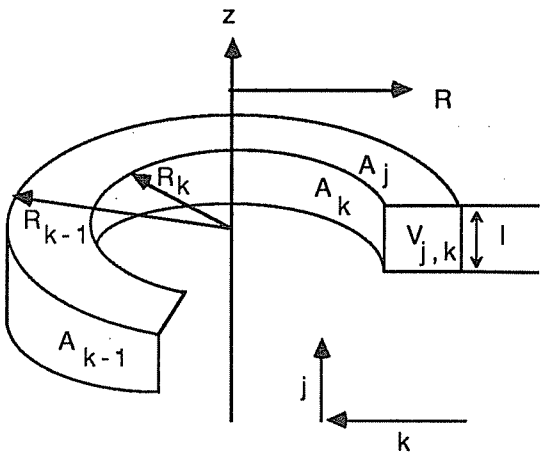

Fig. 1.2. The cylindrical control volume element.

volume element (j,k), which is a ring with inner radius R_k and outer radius R_{k-1}, then applying an energy balance on that volume element results in:

$$\rho V_{j,k}\left.\frac{\partial h}{\partial t}\right|_{j,k} = -kA_k\left.\frac{\partial T}{\partial R}\right|_k + kA_{k-1}\left.\frac{\partial T}{\partial R}\right|_{k-1} + kA_j\left.\frac{\partial T}{\partial z}\right|_j - kA_{j-1}\left.\frac{\partial T}{\partial z}\right|_{j-1} \quad (7)$$

where the surface areas of the element (j,k) are given by

$$A_k = 2\pi R_k l \quad (8)$$

$$A_{k-1} = 2\pi R_{k-1} l \quad (9)$$

and

$$A_j = A_{j-1} = \pi\,(R_{k-1}^2 - R_k^2) \quad (10)$$

and the volume of the element by

$$V_{j,k} = \pi(R_{k-1}^2 - R_k^2)l \quad (11)$$

Using a finite difference approximations for $\delta T/\delta R$ and $\delta T/\delta z$:

$$\left.\frac{\partial T}{\partial R}\right|_k = 2\frac{T_{j,k}^p - T_{j,k+1}^p}{R_{k-1} - R_{k+1}} \quad (12)$$

$$\left.\frac{\partial T}{\partial R}\right|_{k-1} = 2\frac{T_{j,k}^p - T_{j,k-1}^p}{R_k - R_{k-2}} \quad (13)$$

$$\left.\frac{\partial T}{\partial Z}\right|_j = \frac{T_{j+l,k}^p - T_{j,k}^p}{l} \quad (14)$$

and

$$\left.\frac{\partial T}{\partial z}\right|_{j-1} = \frac{T_{j,k}^p - T_{j-l,k}^p}{l} \quad (15)$$

and for $\partial h/\partial_t$:

$$\left.\frac{\partial h}{\partial t}\right|_{j,k} = \frac{h_{j,k}^p - h_{j,k}^{p-1}}{\Delta t} \quad (16)$$

Where the superscript, p, refers to the time level.

Substituting eqns (8–16) into eqn (7), an equation for the enthalpy of a specified element can be written in non-dimensional form. An energy balance on the fluid element results in an equation for the temperature distribution of the fluid element. These two sets of equations can be solved using the Gauss-Seidel iteration method. The detailed analysis of the numerical method used to solve this problem can be found in [4].

4. SYSTEMS DESCRIPTION AND CONTROL STRATEGY

4.1 *Air-based system*[5,6,7]

The transient simulation program TRNSYS[8] is used to determine the performance of the standard solar air space and domestic water system shown in Fig. 2. The parameters selected for the system components are listed in Table 2. The system shown in Fig. 2, has three modes of operation. The first mode occurs when solar energy is available for collection and the space heating load is non-zero. During this mode, the fluid is circulated between the collectors and the load while the storage unit is isolated. The second mode occurs when solar energy is available for collection and the space heating load is zero. In this case, air is circulated between the collectors and the storage unit. The final mode occurs when solar energy is not available for collection and there is a space heating load. In this case, air is circulated between the storage unit and the load. The system operation is controlled by a series of thermostats, fans, and flow diverters. Air flow to the space heating load and auxiliary heat is governed by a two-stage thermostat which monitors room temperature. It commands first stage (solar source) heating when the room temperature drops below 20°C, and second stage (auxiliary source) heating when the room temperature drops below 18.5°C.

4.2 *Water-based system*

The water-based system simulated in this study is shown in Fig. 3, and system parameters are listed in Table 3. This system differs from air-based system in that the storage unit can be charged and discharged simultaneously. This system consists of three independently operating subsystems, i.e. the collector loop, the load, and the domestic hot water system. Whenever solar energy is available, it is collected and transferred to the storage unit. Whenever a space heating load is present, it is met by the storage unit and the auxiliary energy source. The domestic hot water system takes energy from the storage unit when it is necessary. Relief valves are shown for dumping excess energy.

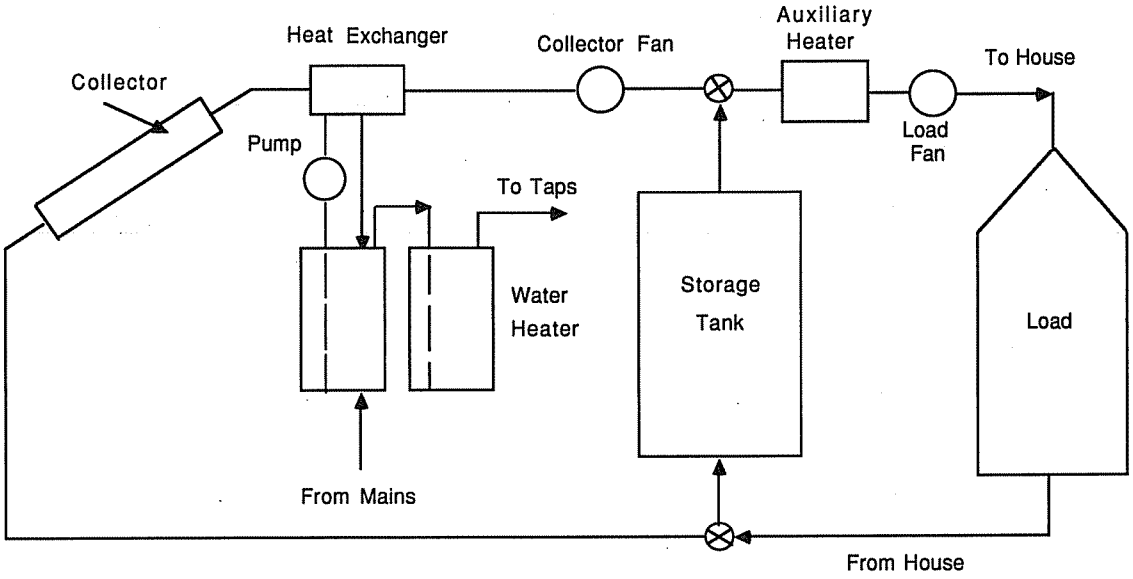

Fig. 2. Schematic representation of the standard solar air heating system.

5. RESULTS AND DISCUSSION

5.1 *Air-based system*

The effect of storage capacity on system performance for the air-based system using wax (PCES) are shown in Fig. 4. These results are obtained from one week of simulation starting January 1 in Albuquerque, NM. The pebble bed used the same computer program as used for PCES by setting the material melting temperature arbitrarily high, so that all energy stored is in the form of sensible heat. For sensible heat storage with the infinite NTU assumption, the model reduces to that developed by Hughes *et al.*[9]. Figure 4 shows the difference between the present finite NTU model and the infinite NTU model used by Morrison *et al.* for the parameters values investigated. There is a little difference between the finite and infinite NTU results (less than 2% at the smallest storage mass used 5 kg/m^2, corresponding to NTU = 1. As storage capacity increases (which increases the value of NTU for the finite NTU model), this difference becomes smaller and approximately disappears completely at storage capacities above 40 kg/m^2 (corresponding to NTU = 8). These results indicate that for air-based systems the infinite NTU can be used with a very small error taking advantage

Table 2. Air-based system

Collector		**Load**	
Number of glass covers	2	Load capacitance (MC_P)	20,000 kJ/K
Product of extinction coefficient and thickness of each glass cover	0.037	Nominal space heating load (UA)	1000 kJ/h K
Refractive index	1.526	Water preheat tank volume	0.35 m^3
Collector plate absorptance (α)	0.95	Air to water heat exchange effectiveness	0.75
Collector emittance (ϵ)	0.9	Cold water inlet	15°C
Collector efficiency factor ($\acute{F}$)	0.7	Set point for hot water	60°C
Back and side losses	1.5 kJ/h m^2 K		
Mass flow rate per unit collector area	44 kg/h m^2		
Glazing spacing	0.04 m		

Ducts

The collector circuit pipings and the heating circuit piping are divided into a cold and a hot side, and the following data are the same for both sides.

Collector circuit pipe (each side)		**Heating circuit pipe (each side)**	
Length	20 m	Length	15 m
Diameter	0.04 m	Diameter	0.04 m
Heat loss	20 kJ/h K	Heat loss	15 kJ/h K
Fluid density	1.204 kg/m^3	Fluid density	1.204 kg/m^3
Fluid specific heat	1.012 kJ/kg K	Fluid specific heat	1.012 kJ/kg K
Ambient temperature	20°C	Ambient temperature	20°C

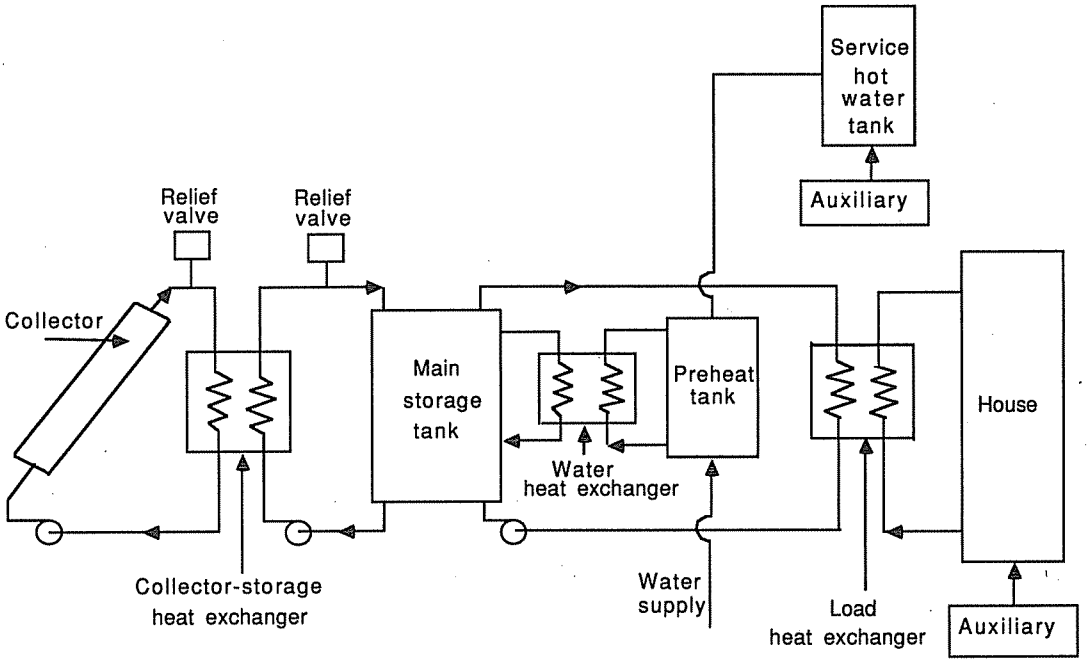

Fig. 3. Schematic representation of solar water heating system.

of its huge decrease in computational cost in comparison with the finite NTU model. Further results were obtained for the air-based system using the infinite NTU model. The following results are generated using one year simulation in Albuquerque. Figures 5 and 6 show the variation of solar fraction with storage mass and storage volume for sodium sulphate decahydrate, paraffin wax (P116), and medicinal paraffin. The first two materials were studied by Morrison *et al.* The third was chosen because it has a semicongruent melting behavior over a temperature range of 40–44°C. At a solar fraction equal to 0.85, Morrison *et al.* recommend storage capacities of 12 kg/m^2, 16 kg/m^2, 118 kg/m^2 for $Na_2SO_4.10H_2O$, paraffin wax, and pebble bed storage, respectively. A system using sodium sulphate and wax will require only 17%, and 40% of the storage volume of a pebble bed system to achieve the same system performance. At the same solar fraction (0.85), the values resulting from the more detailed model in this study are 14 kg/m^2, 17 kg/m^2, 23 kg/m^2, and 125 kg/m^2 for sodium sulphate decahydrate, P116 wax, medicinal paraffin, and pebble bed, respectively. The present storage capacities are slightly higher than those indicated by Morrison *et al.* for sodium sulphate and paraffin wax due to the effect of storage energy losses. The storage volume required for medicinal paraffin is slightly larger than the storage volumes required

Table 3. Water-based system parameters

Collector		**Collector circuit pipe (each side)**	
Number of glass covers	2	Length	20 m
Product of extinction coefficient and thickness of each glass cover	0.037	Diameter	0.05 m
Refractive index	1.526	Heat loss	18 kJ/h K
Collector plate absorptance (α)	0.95	Fluid density	1000 kg/m^3
Collector emittance (ϵ)	0.9	Fluid specific heat	4.197 kJ/kg K
Collector efficiency factor ($\acute{F}$)	0.9	Ambient temperature	20°C
Back and side losses	1.5 kJ/h m^2 K		
Mass flow rate	50 kg/h m^2		
Piping			
The collector circuit piping and heating circuit piping are divided into a cold side and a hot side, and the following data are the same for both.			
Heating circuit pipe (each side)		**Preheat tank**	
Length	15 m	Volume	0.35 m^3
Diameter	0.05 m	Thermal loss	1.5 kJ/h m^2 K
Heat loss	10.8 kJ/h K	Shape	H/D = 1
Fluid density	1000 kg/m^3	Cold water inlet temperature	15°C
Fluid specific heat	4.197 kJ/kg K	Ambient temperature	20°C
Ambient temperature	20°C	Set point for hot water	60°C

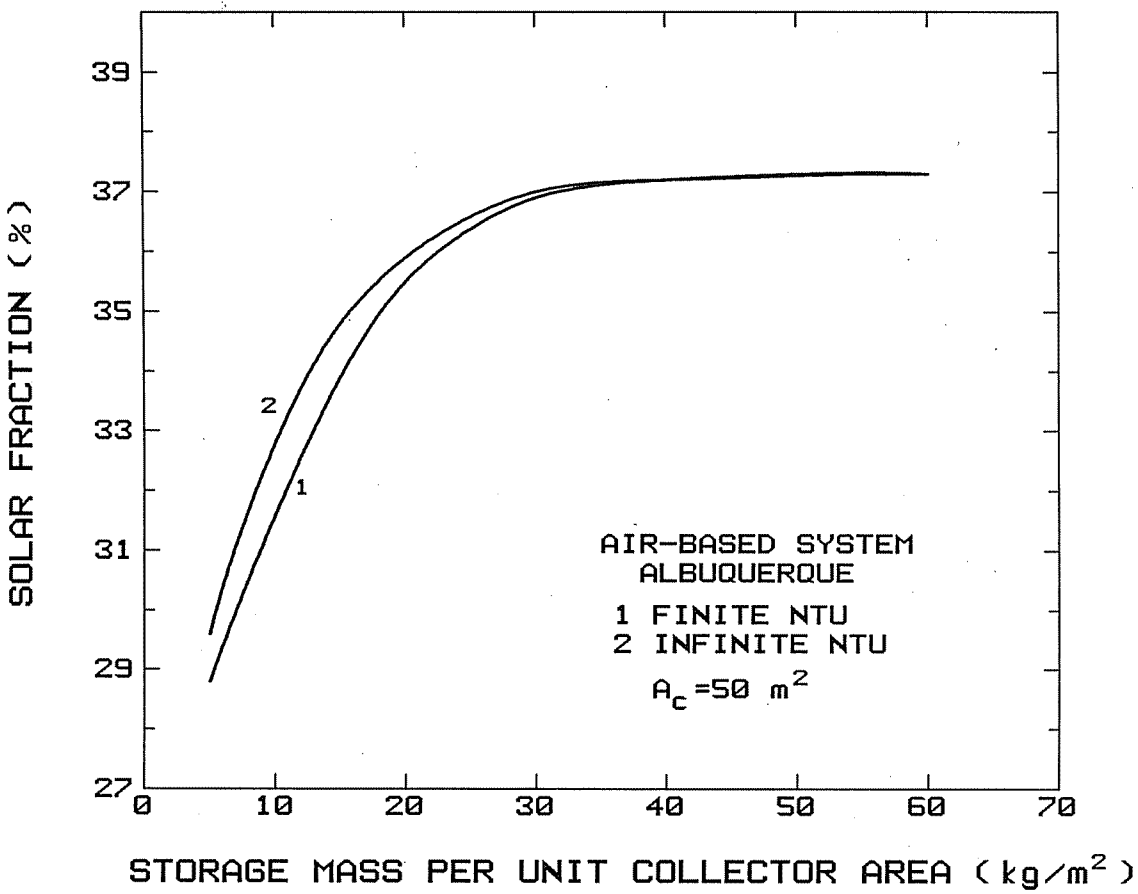

Fig. 4. Variation of solar fraction with storage mass for P116 WAX (one week simulation starting January 1).

for sodium sulphate and paraffin wax because it has the lowest latent heat (146 kJ/kg) and a relatively high melting temperature (40–44°C). Systems using sodium sulphate, P116 wax, and medicinal paraffin will require roughly 18%, 40%, and 51% of the storage volume of sensible heat system using pebbles in order to achieve the same system performance. These results indicate the advantage of using phase-change material. The results presented here are based on ideal behavior of the PCM, because such phenomena as property degradation, supercooling, and crystallization are not accounted for.

5.2 *Water-based systems*

For water-based systems, a parametric study for energy stored was conducted because significant differences between the finite and infinite NTU models were expected due to the relatively large heat capacity of water. Figure 7 shows the variation of fluid outlet temperature with time for P116 wax at different values of NTU. These figures have been generated for constant inlet fluid temperature (T_{fi} = 80°C) during the heating mode only. As the NTU increases at a given time, the outlet fluid temperature becomes smaller (i.e., more heat is removed from the fluid and consequently more heat will be stored in the material). This figure shows that there is a significant difference between the finite and infinite NTU model. In the following analysis, when axial conduction is considered it will be called the one-dimensional (1D) finite NTU model, and when both axial and radial conduction are considered, it will be called the two-dimensional (2D) finite NTU model. Figure 8 shows the variation of stored energy with time for P116 wax. There is little difference between the finite NTU model 1D, and the finite NTU model, 2D but still there is a significant difference between the values of stored energy obtained using the infinite NTU model and the finite NTU model about 36%. The effect of both the number of radial points (N) and the number of axial points (M) on the stored energy for wax were studied. There is no significant variation in the stored energy with increasing the number of radial points above 5 (i.e., N = 5) or with increasing the number of axial points above 10 (i.e., M = 10). A comparison was made between using the finite NTU, 1D, and the finite NTU, 2D in Fig. 9 for P116 wax. As seen from figure, the 2D model gives slightly better results and the difference between the two models becomes smaller as the NTU increases, and disappears for NTU values above 100. This behavior is due to many factors such as the amount of mass flow

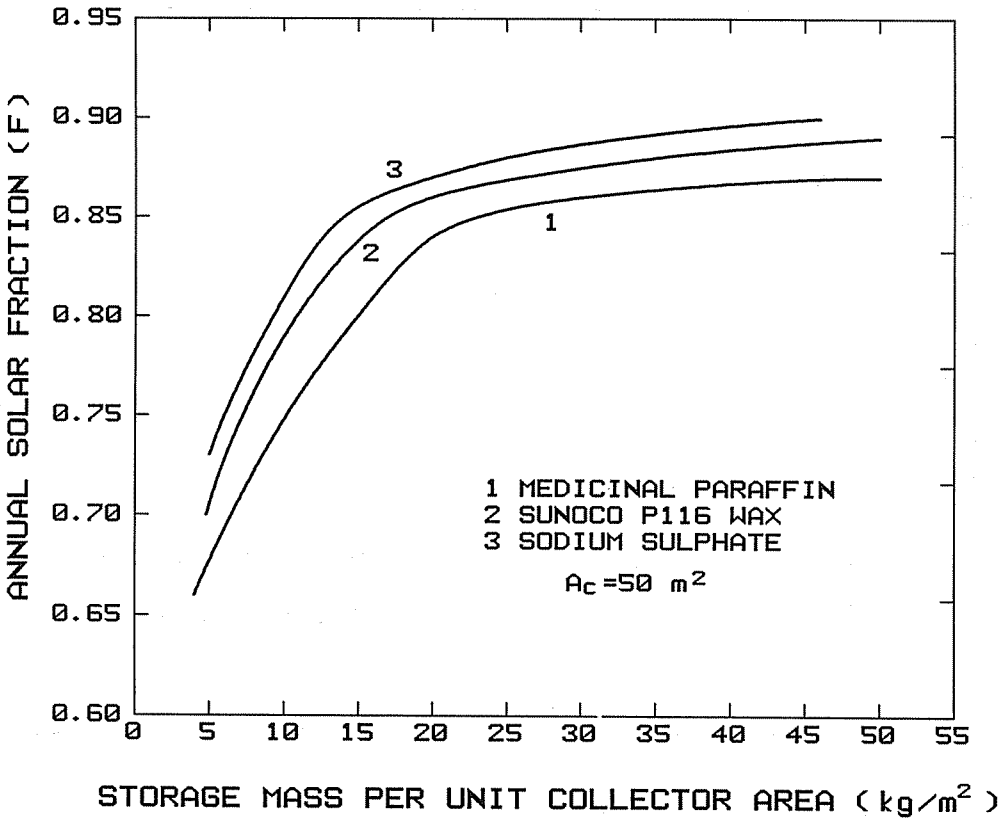

Fig. 5. Variation of solar fraction with storage mass for air-based system in Albuquerque, NM.

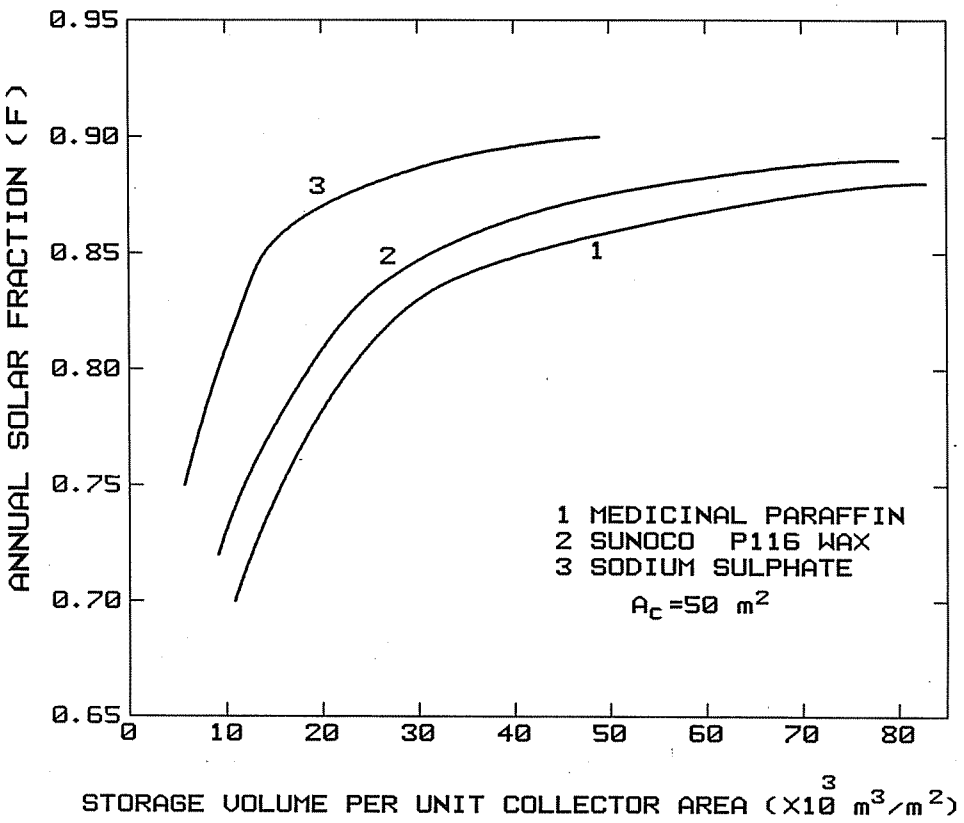

Fig. 6. Variation of solar fraction with storage volume for air-based system utilizing sensible and latent heat storage media in Albuquerque, NM.

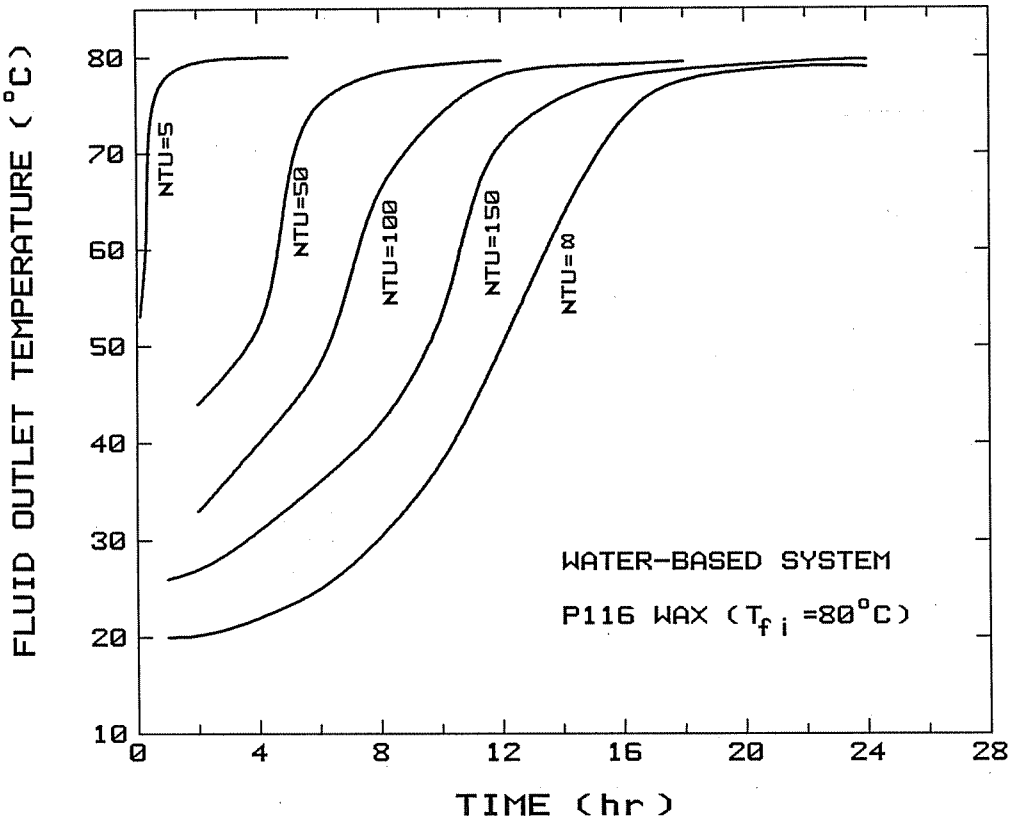

Fig. 7. Variation of outlet fluid temperature with different values of NTU for P116 WAX.

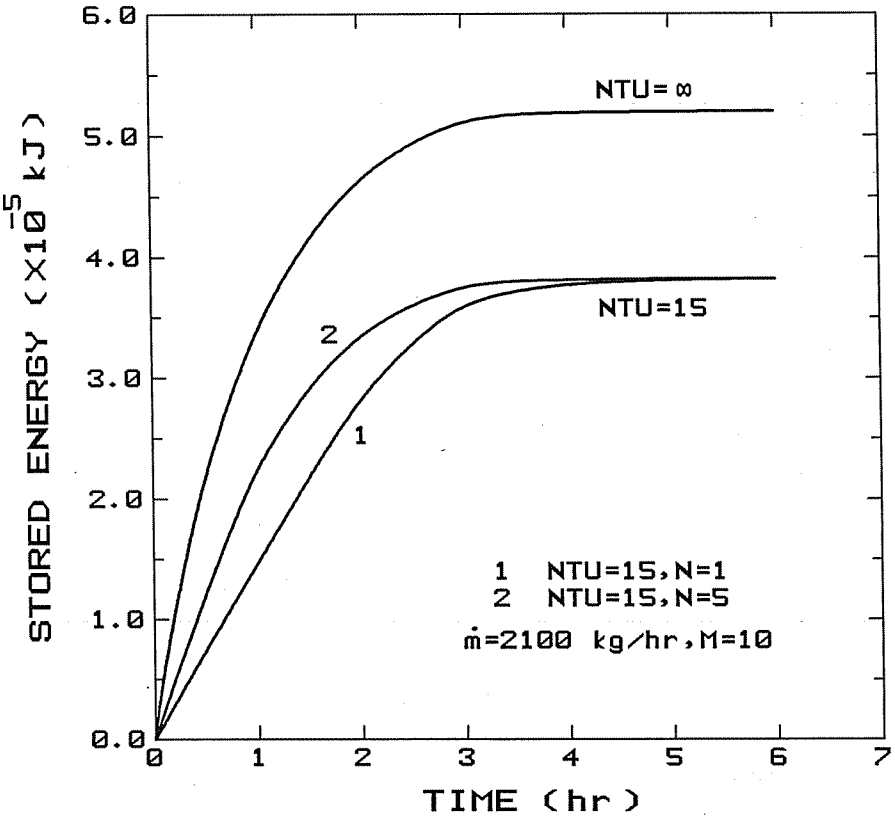

Fig. 8. Variation of stored energy with time, for P116 WAX (water-based system).

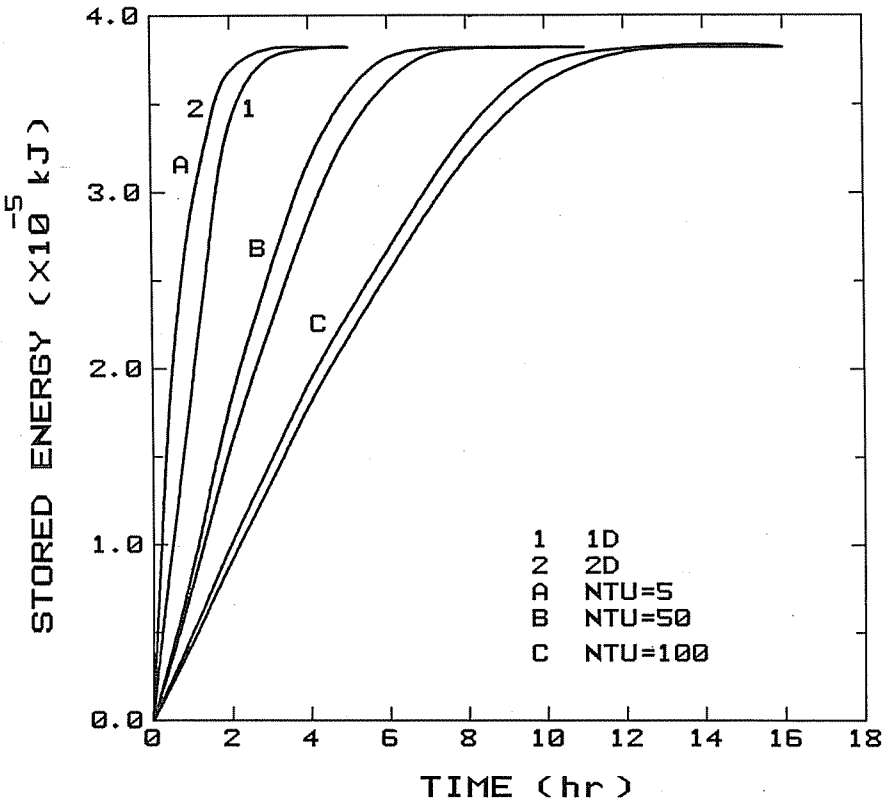

Fig. 9. Comparison between 1D and 2D for P116 WAX (latent-heat storage) with water-based system.

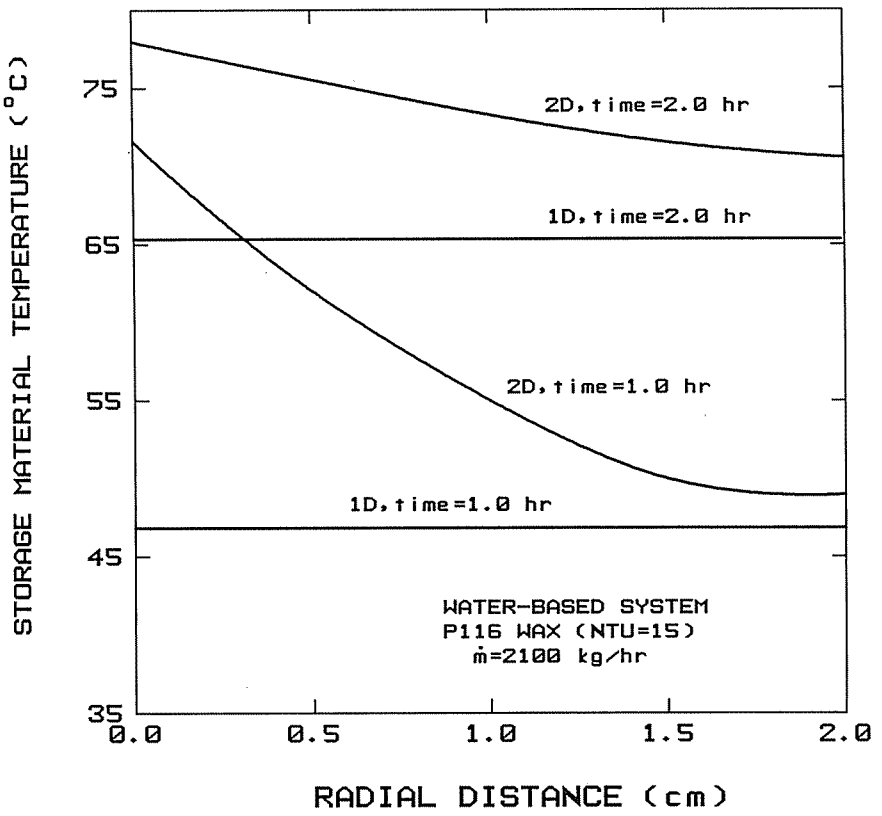

Fig. 10. Variation of storage material temperature with radial distance (measured from material surface).

rate, system size, inlet fluid temperature, heat transfer coefficient between the fluid and material surface, fluid temperature distribution, and storage material temperature distribution. Since the stored energy in the material depends on the area under the temperature versus distance curve, the result for the more accurate 2D case is due to the increase in this area when considering the temperature gradients in the storage material. Figure 10 shows the variation of the storage material temperature with the radial distance for P116 wax for different times of heating the storage unit (T_{fi} = 80°C, and $\dot{m}$ = 2500 kg/h). This figure shows that the area under the curves is larger for the 2D case.

To study the effect of different models on the values of solar fraction, the standard water-based system shown in Fig. 3 was simulated, using both PCES and a stratified conventional water tank (5 nodes) for the main storage tank. The simulation was run in Albuquerque for one week starting January 1. To examine this effect, consider a solar fraction of 0.65. From Fig. 11, the recommended storage masses per unit collector area are 13.5 (0.025), 16 (0.029), and 18 kg/m^2 (0.033 m^3/m^2) for infinite NTU model, finite NTU (2D), and finite NTU model (1D) respectively. So, the use of infinite NTU model of Morrison *et al.* will give an error in solar fraction value of about 14%, whereas the difference between finite 1D, 2D models values is roughly 4%. An accurate examination of the water-based system can be obtained only using the exact solution, i.e., the finite NTU (2D) model. The approximation of infinite NTU model (unlike in the air-based system) gives a significant error in the determination of the system performance. Figure 12 shows the variation of solar fraction with storage volume for water tank, P116 wax, and sodium sulphate. Here, the reduction in storage volume is not so pronounced as the case of air-based system. For example, a solar fraction of 0.65 can be realized by using a sodium sulphate with a storage volume of 0.014 m^3/m^2 (14 kg/m^2) or a paraffin wax with a storage volume of 0.029 m^3/m^2 (16 kg/m^2) or a conventional water tank with a storage volume of 0.029 m^3/m^2 (29 kg/m^2), i.e., the required storage volume of sodium sulphate is roughly 50% of the storage volume required by a conventional water tank to realize the same system performance. For paraffin wax, the storage volume required is the same as required by a conventional water tank. So even with liquid-based system, use of phase-

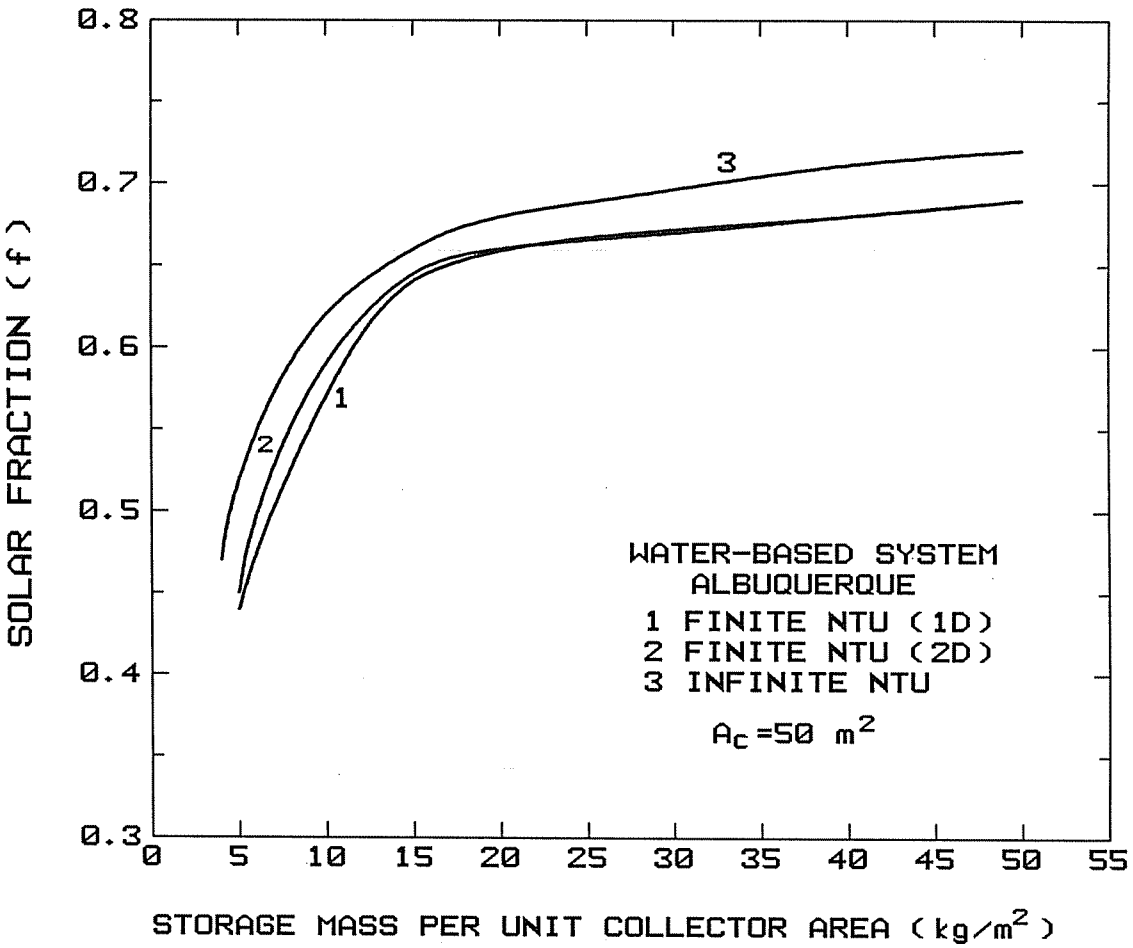

Fig. 11. Variation of solar fraction with storage mass for P116 WAX (one week simulation starting January 1).

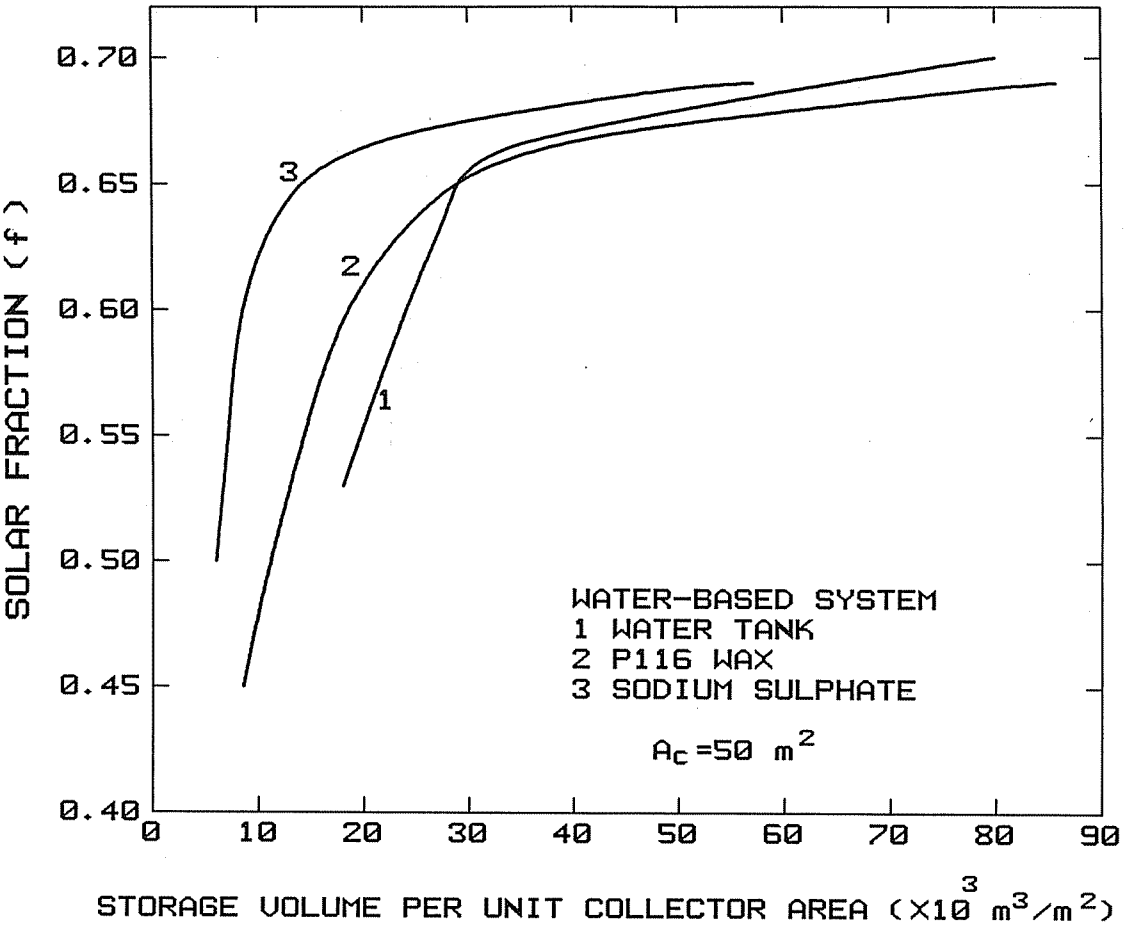

Fig. 12. Variation of solar fraction with storage volume for sensible and latent heat storage media in Albuquerque, NM.

change material can result in a decrease in the storage volume but not nearly as large as in the air-based system. The recommended value for the storage volume for P116 wax (i.e., the value of storage volume above which there is no significant increase in system performance—0.03 m^3/m^2) for air-based system is approximately equal to the recommended value for water-based system (0.029 m^3/m^2). The recommended storage volume does not depend on system configuration, i.e. air-based or water-based system for any of the materials studied.

NOMENCLATURE

- A cross-sectional area
- A_c collector area
- A_t inside surface area of the storage tank
- c_f specific heat of circulating fluid
- c_s specific heat of PCM in solid phase
- c_l specific heat of PCM in liquid phase
- F annual solar fraction
- f solar fraction
- H^* non-dimensional enthalpy
- h specific enthalpy
- h_{sl} latent heat (solid–liquid transition)
- k thermal conductivity
- k_s thermal conductivity of PCM in solid phase
- k_l thermal conductivity of PCM in liquid phase
- L storage unit length
- l axial length of control volume element
- M number of axial elements
- M_s storage mass
- $\dot{m}$ mass flow rate
- N number of radial elements
- N_c number of cylinders
- NTU number of transfer units $\left(NTU = \dfrac{U P L}{\dot{m} c_f}\right)$
- P perimeter of the storage material ($P = 2\pi R_c N_c$)
- R radial distance
- R_c radius of the cylinder
- T temperature
- T_{fi} inlet fluid temperature
- T_{fo} outlet fluid temperature
- T_{m1} lower melting temperature
- T_{m2} upper melting temperature
- t time
- U total loss heat transfer coefficient
- $V_{j,k}$ control element volume
- V_t the inside volume of the storage tank
- z axial distance
- ΔT_m transition range width
- θ non-dimensional temperature
- ρ PCM density

Acknowledgments—The author would like to express appreciation to Professor J. A. Duffie, Director of Solar Energy Laboratory at the University of Wisconsin-Madison for allowing use of the Solar Laboratory facilities. Profes-

sor S. A. Klein deserves much of the credit for his guidance and useful suggestions. Useful discussions with members of the Solar Laboratory, in particular those of James Braun are appreciated. Great help by TRNSYS Engineer Jim Kummer in solving TRNSYS' problems is acknowledged. The financial support of Egyptian Government during this study is appreciated.

REFERENCES

1. D. J. Morrison and S. I. Abdel Khalik, Effect of phase-change energy storage on the performance of air-based and liquid-based solar heating systems. *Solar Energy* **20,** 57–67 (1978).
2. J. J. Jurinak and S. I. Abdel Khalik, On the performance of air-based solar heating systems utilizing phase-change energy storage. *Solar Energy* **24,** 503–522 (1979).
3. D. Hale, M. Hoover, and M. O'Neill, Phase Change-Materials Handbook, NASA CR–61363, NASA George C. Marshall Space Flight Center (1971).
4. H. Visser, Energy storage in phase-change materials-development of a component model compatible with TRNSYS. Final report, contract No. 2462–84–09 ED ISPNL, Delft Univ. of Technology, Department of applied physics, Delft (1986).
5. J. A. Duffie, and W. A. Beckman, Solar energy thermal processes. Wiley Interscience, New York (1980).
6. W. Beckman, S. Klein, and J. Duffie, Solar heating design by the F-chart method. Wiley Interscience, New York (1977).
7. H. P. Garg, Advances in solar energy technology, vol. 2, D. Reidel Publishing Company, Holland (1987).
8. S. A. Klein, *et al.*, TRNSYS: A transient simulation program, University of Wisconsin-Madison, version 12.1 (1983).
9. P. J. Hughes, S. A. Klein, and D. J. Close, Packed bed thermal storage models for solar air heating and cooling systems. Trans. ASME, J. Heat transfer **98,** 336 (1976).